Supporting Information

Nadel et al. 10.1073/pnas.1302277110

SI Text

S1. Micromorphological and Scanning Electron Microscope/Energy Dispersive X-Ray Spectroscopy Analyses

Materials and Methods. To characterize depositional and postdepositional processes at the site in general and the graveyard in particular, we retrieved 74 samples for micromorphological analyses. These samples were collected from all types of loci. So far we have analyzed 29 samples: 14 samples from the graveyard in the first chamber (some Natufian burial pits were dug into earlier Natufian graves and sediments, several were dug into Middle Paleolithic sediments, and the bottom ones are located directly on limestone bedrock), 11 samples from bedrock mortars in the first chamber and on the terrace, and four samples from tufas and rock crusts (1, 2).

The 29 samples were collected as undisturbed blocks. All samples were processed in the Laboratory of Geology at the University of Haifa. They were impregnated with a polyester resin/styrene mixture under vacuum, dried, and cut into small cubes. Then petrographic thin sections (30 μm thick) were sliced off in the petrography laboratory of the Department of Maritime Civilizations at the University of Haifa. The thin sections were examined with Olympus BH-2 petrographic microscope in plane-polarized (PPL) and cross-polarized (XPL) light using magnifications of 40× to 400×. They are described according to Stoops' method (3), applying concepts accepted in micromorphology of archaeologically related sediments (4, 5). The microstructure and chemical composition studies were performed on a Quanta scanning electron microscope (SEM), Oxford Instruments FEA, linked with an energy-dispersive spectrometer (EDS) INCA 200, in the Materials and Environmental Engineering Department of the Technion-Israel Institute of Technology. The SEM/EDS samples were analyzed uncoated, and all SEM microphotographs were taken in the mode of back-scattered (BS) electrons.

Results. The burial pits were filled during the inhumation process with ash-rich deposits mixed with local soil materials (Fig. S5). The thin-section analyses indicate that bioturbation was common in the upper deposits of the graveyard and decreased substantially downward. Moreover, the articulation of the skeletons and the associated in situ artifacts (e.g., stones set on edge, flint cores near the skulls, selected animal bones in particular locations) clearly reflect contextual preservation of macroscopic remains. Combined with the microscopic studies, the Raqefet Cave burials serve as excellent examples where not only the skeletons and their associated durable material remains were preserved intact but even perishable materials—the impressions of plant linings—were preserved at the bottom of graves. The high phytolith densities in burials and bedrock mortars indicate good preservation conditions as well as distinct and common use of plants in both (see below). Overall, the variety of remains and observations, combined with thin-section analyses, establish that bioturbation and other postdepositional processes had little impact on the location of anthropogenic artifacts within graves or bedrock mortars.

S2. Phytolith Analysis

Materials and Methods. Because macroscopic botanical remains are extremely scarce in the southern Levantine Natufian sites (6, 7), phytolith analyses provide one of the few possible direct ways to reconstruct past plant-related activities. To study plant use through the spatial distribution of phytoliths at Raqefet Cave, we analyzed 35 sediment samples retrieved from all types of in situ Natufian features. These samples include 16 samples from eight inhumations, 12 samples from four bedrock mortars, two samples from a deep bedrock basin above which there were three burials, and two samples from Natufian tufa; we also studied a pre-Natufian (Kebaran) tufa and two control samples taken from naturally accumulating soils located 40 m and 100 m from the cave's entrance (Table S2).

The sediment samples were analyzed by R.C.P. at the Institute of Archaeology (University College London, London, United Kingdom) and the Plant Foods Research Group (Max Planck Institute for Evolutionary Anthropology, Liepzig, Germany). Phytoliths were extracted following a conventional protocol using gravity sedimentation, dry-ashing, and heavy liquid floatation (8). These phytoliths were treated with 15 mL of 10% HCl to remove any calcium carbonates. HCl then was removed by centrifuging. Clays were dispersed by adding 20 mL of a 5% solution of sodium hexametaphosphate and distilled water in a cylinder. Water then was added to a height of 8 cm. After 70 min the water was poured off, and the cylinder was refilled with water, which was left to settle for 60 min and then was poured again. This process was repeated until the suspension was clear. The organic matter in the residue was removed by heating to 500 °C in a muffle furnace for 2 h. The samples were transferred into 15-mL centrifuge tubes. Then 3 mL of sodium polytungstate solution calibrated to 2.3 specific gravity was added to each tube. The sample was centrifuged at 115–120 × g for 10 min. The tubes were removed, and the suspension containing the phytoliths was poured into clean 15-mL tubes. Distilled water was added to the tubes to reduce the specific gravity, and then the tubes were centrifuged at 721–752 × g for 5 min. After two such treatments, the clean phytoliths were transferred into beakers, dried, and weighed. Entellan (Merck) or Permount (Fisher) was used to mount a weighed aliquot of 2–3 mg of residue from each sample. A wide variety of plant tissue and taxa were identified (Table S3). Phytolith counting was conducted at 400× magnification. Single-cell phytolith morphotypes were counted to 300 or more individuals. Because multicell phytoliths are composed of varying numbers of cells, they were tallied separately. Multicell forms were counted up to 100. The number of phytoliths on the slide was calculated using the following algorithm:

$$\mathbf{n\ phytoliths\ per\ slide} = \mathbf{n\ counted}/\mathbf{n\ slide\ fields\ counted} \times \mathbf{total\ n\ fields\ on\ slide}.$$

This value was used to derive a comparable unit of quantification, the number of phytoliths per 1 g of sediment. This value was calculated with the following formula:

$$\mathbf{n\ phytoliths}/\mathbf{g} = \mathbf{n\ phytoliths\ per\ slide}/\mathbf{total\ amount\ of\ sediment\ mounted\ (mg)} \times \mathbf{total\ phytolith\ amount\ (mg)}/\mathbf{total\ initial\ sediment\ (mg)} \times \mathbf{1,000}.$$

We used this formula and an Excel spreadsheet (Microsoft) to calculate the number of each phytolith type on each slide and the number of each type per gram (<0.25 mm) of dry sediment.

Results. Control samples taken from outside the cave and in various contexts inside the cave indicate that jigsaw-puzzle phytoliths were rare outside the burial contexts (Table S4). Controls show low levels of all phytoliths and extremely low levels of dicot leaf

phytoliths. This finding verifies that the presence of dicot phytoliths is the result of cultural practices associated with burials and not the result of natural processes or contamination. The high correlation between the burials and dicot phytoliths is apparent in the burials of Homo 18 and Homo 19, where a set of well-preserved plant impressions was preserved on a vertical chiseled surface (Fig. S4). This finding implies an association between dicot leaf phytoliths and plant impressions in certain burial contexts.

1. Nadel D, et al. (2008) The Late Natufian at Raqefet Cave: The 2006 excavation season. *J Isr Prehist Soc* 38:59–131.
2. Nadel D, et al. (2012) The 2010 and 2011 seasons of excavation at Raqefet Cave. *J Isr Prehist Soc* 42:35–73.
3. Stoops G (2003) *Guidelines for Analysis and Description of Soil and Regolith Thin Sections* (Soil Science Society of America, Madison, WI).
4. Courty M-A, Goldberg P, Macphail RI (1989) *Soils and Micromorphology in Archaeology. Cambridge Manuals in Archaeology* (Cambridge Univ Press, Cambridge, UK).
5. Goldberg P, Macphail RI (2006) *Practical and Theoretical Geoarchaeology* (Blackwell Publishing, Oxford, UK).
6. Rosen AM (2010) Natufian plant exploitation: Managing risk and stability in an environment of change. *Eurasian Prehistory* 7:117–131.
7. Rosen AM, Rivera-Collazo I (2012) Climate change, adaptive cycles, and the persistence of foraging economies during the late Pleistocene/Holocene transition in the Levant. *Proc Natl Acad Sci USA* 109(10):3640–3645.
8. Rosen AM (1999) in *The Practical Impact of Science on Aegean and Near Eastern Archaeology*, eds Pike S, Gitin S, Wiener Laboratory Publication 3 (Archetype, London), pp 86–92.

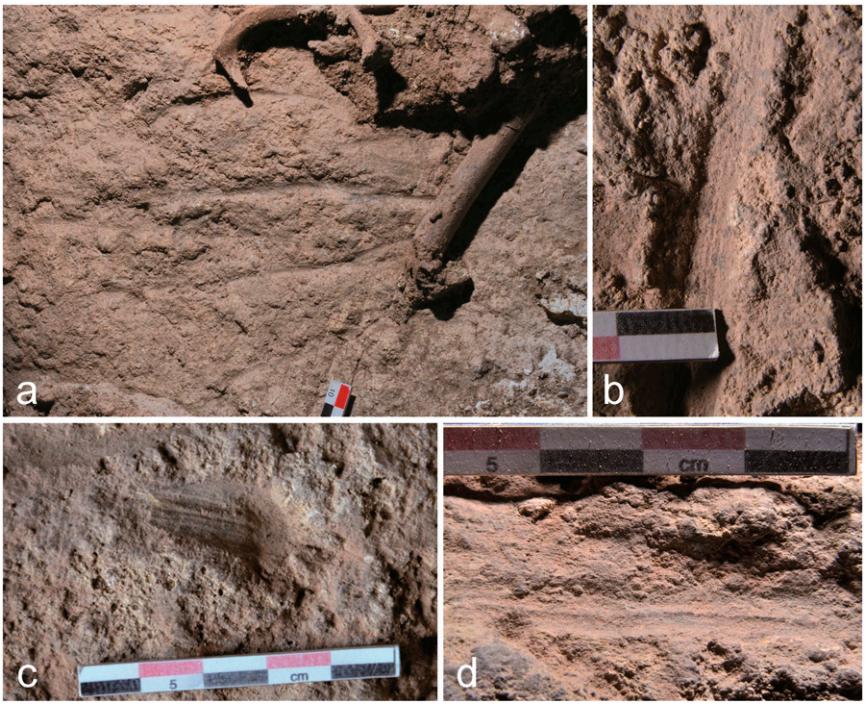

Fig. S1. Field photographs of stem impressions. All scales are in centimeters. (*A*) Bones of Homo 31, a 6- to 8-y-old child, directly above impressions of round stems. (*B–D*) Close-up views of rectangular stem impressions in the grave of Homo 25 and Homo 28. Photographs reproduced with permission from E. Gernstein.

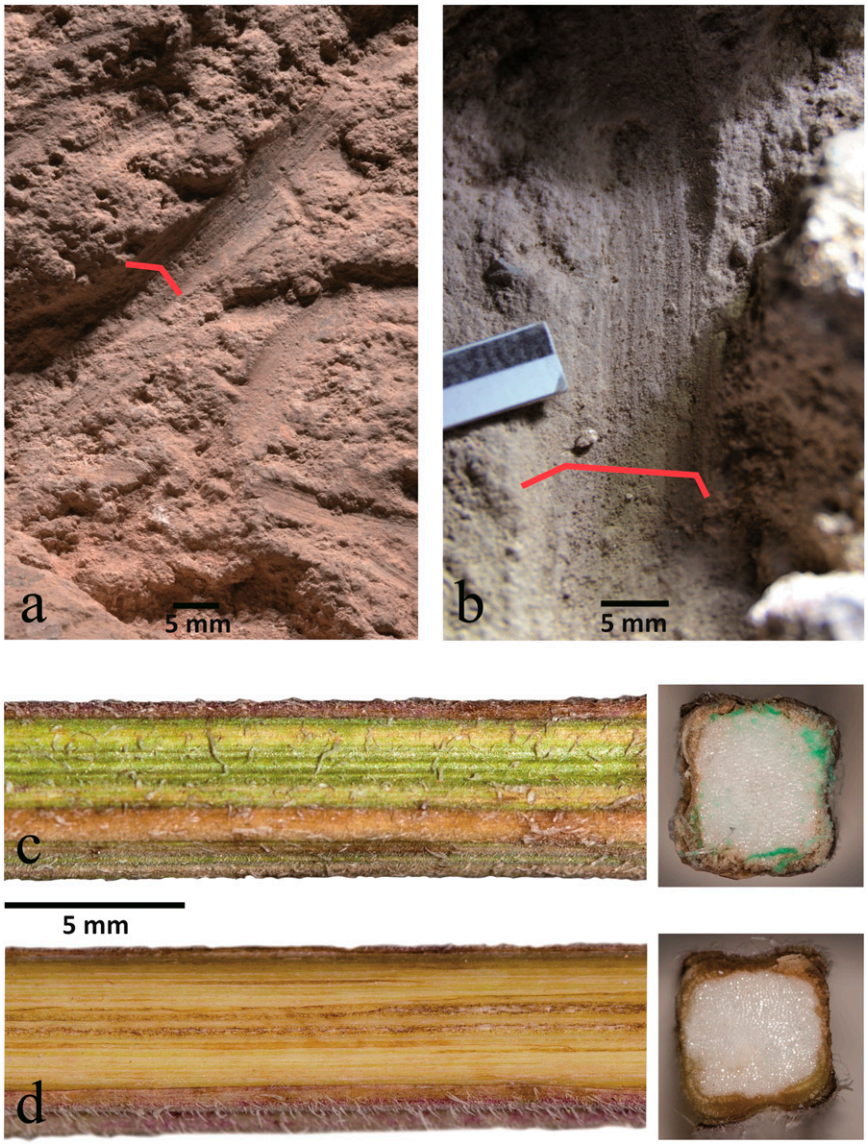

Fig. S2. (*A* and *B*) Field photographs of stem impressions in the graves of Homo 25 and Homo 28. The impressions are rectangular in cross-section, as marked by the red line. Photographs reproduced with permission from E. Gernstein. (*C*) Photographs of a stem segment and its rectangular cross-section (*Salvia judaica*). (*D*) Photographs of a stem segment and its rectangular cross-section (*Salvia fruticosa*). Both *Salvia* species currently grow near Raqefet Cave. Photographs in *C* and *D* reproduced with permission from M. Eisenberg.

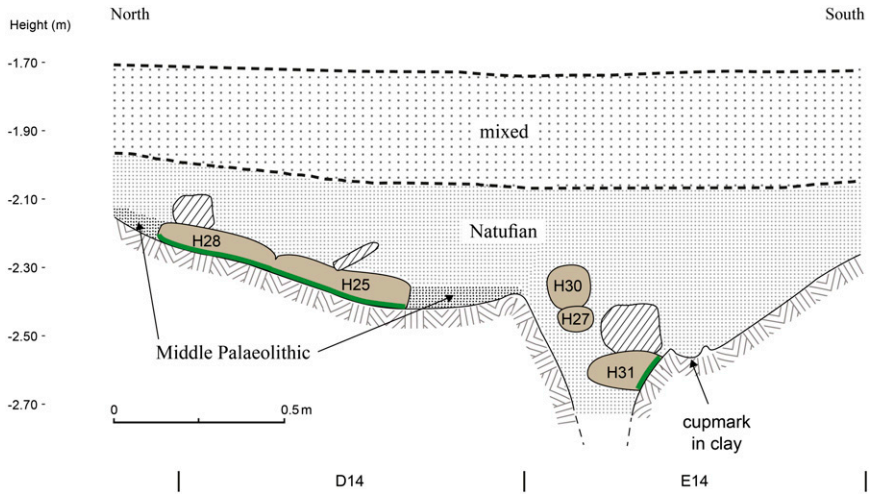

Fig. S3. A section through selected burials discussed in text; see Fig. 1*C* for location. The presence of plant impressions on a mud veneer is indicated by the green line at the bottom of two graves. Note stones set on edge on top of Homo 28, Homo 25, and Homo 31 (diagonal hatching). The slab on the chest of Homo 25 is in addition to the one set near its skull (to the west of this section, not presented here; see Fig. 2). The shallow pit for the double burial on the left was dug through a Middle Paleolithic layer, down to bedrock. Homo 27 and Homo 30 are only partially preserved.

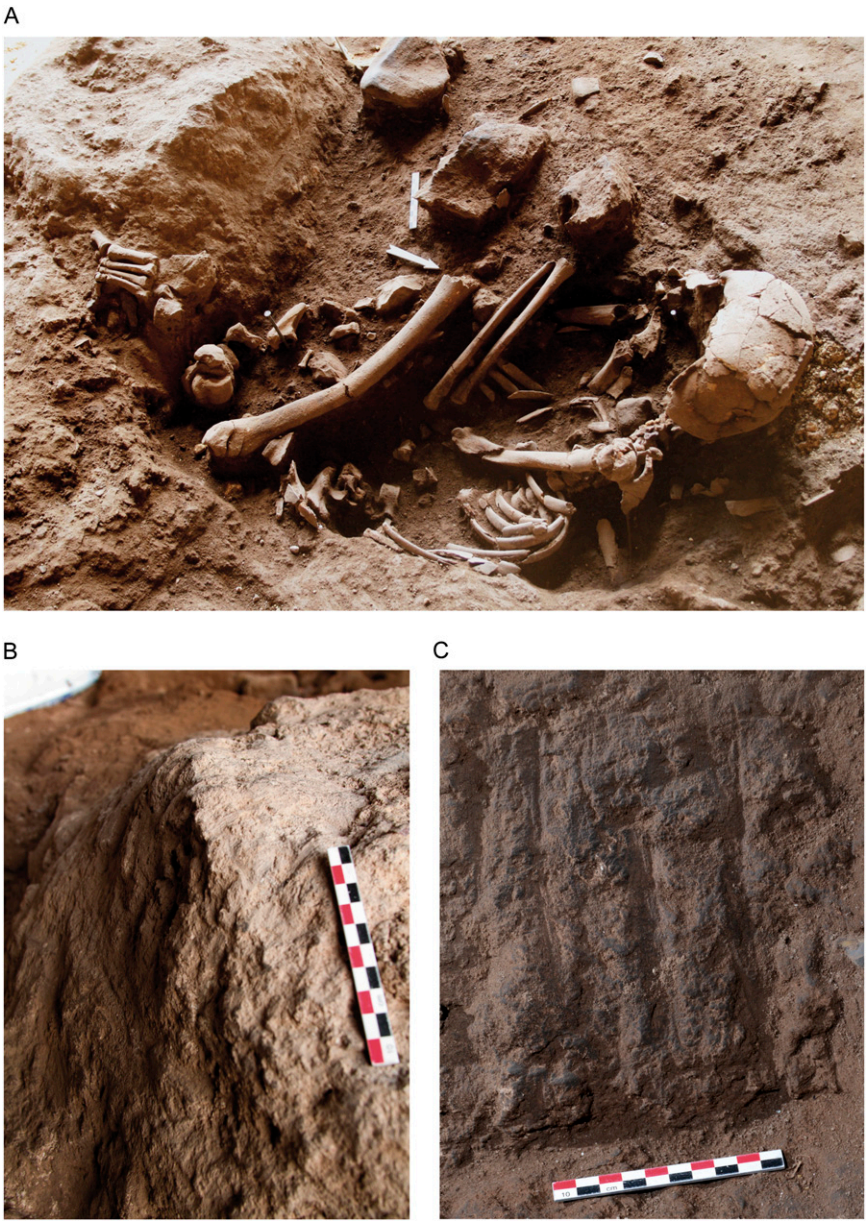

Fig. S4. The double burial of Homo 18 and Homo 19 (see location in Fig. 1*C*). (*A*) Homo 19 during excavation (skull on right). Note the vertically chiseled bedrock surface at the left with foot bones resting on it. This surface was covered by more than 10 plant impressions. Photograph reproduced with permission from E. Gernstein. (*B*) An opposite view of the chiseled surface, after removal of the skeleton. Photograph reproduced with permission from E. Bartov. (*C*) A close-up view of plant impressions found on the vertical chiseled surface. All scales are in centimeters. Photograph reproduced with permission from E. Gernstein.

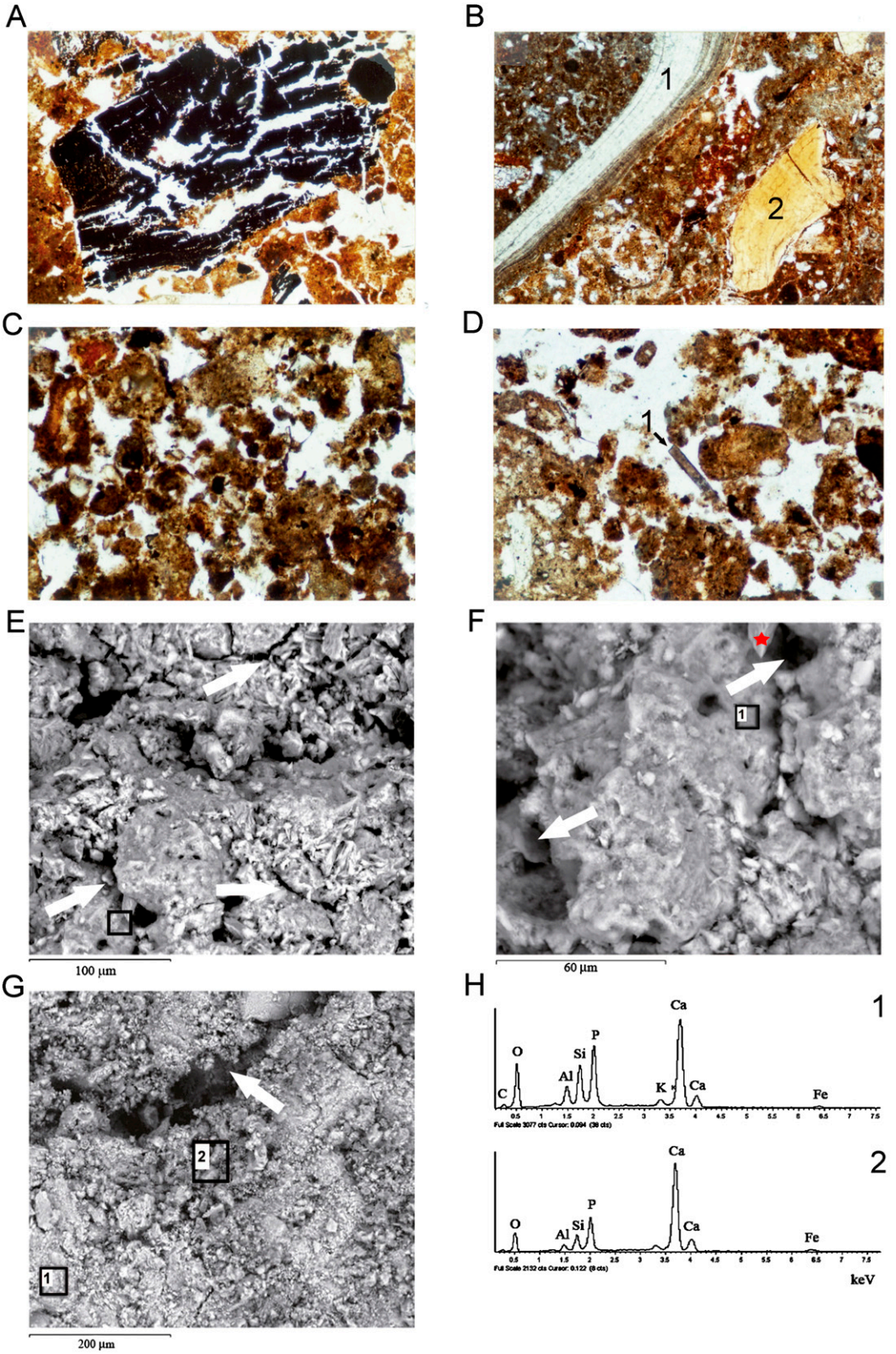

Fig. S5. (*A*) Sample 3, the top of Locus 1: partially fragmented charcoal specimen from a hearth embedded in the clayey anthropogenic deposit; PPL, width of frame 2.4 mm. (*B*) Sample 4, the top of Locus 1: heterogenic ash-derived deposit encompassing a land snail shell fragment (1) and a yellow chip of bone (2); PPL, width of frame 2.4 mm. (*C*) Sample 5, Locus 1: fill of the burial of Homo 9, a loose anthropogenic deposit comprising pulverized small, rounded organo-mineral aggregates; PPL, width of frame 0.98 mm. (*D*) Sample 6, Locus 1, fill of the burial of Homo 9, a channel filled with comminuted organo-mineral aggregates and an elongated phytolith (1); PPL, width of frame 0.98 mm. (*E*) Sample Raq-11–1, floor of burial Homo 25 and Homo 28: back-scattered image of fractured (arrows), mainly amorphous mass of a crust. (*F*) Close-up view of *E*. Square denotes area measured by EDS, arrows indicate rounded pores, asterisk shows tip of

Legend continued on following page

idiomorphic hydroxyapatite crystal probably grown on parent calcite. (*G*) Sample Raq-11–1, floor of burial Homo 25 and Homo 28: Back-scattered image of heterogeneous crust surface dissected with fracture (arrow); note bright area (square 1, phosphate mineral phase) vs. darker area (square 2, alumosilicate phase). (*H*) EDS graphs of elemental composition in squares 1 and 2 in *G*. Major peaks of calcium and phosphorus are related to a phosphate phase, whereas silicon, aluminum, potassium, and iron are related to a silicate phase. Parts *A–B* and *E–H* reproduced with permission from The Israel Prehistoric Society.

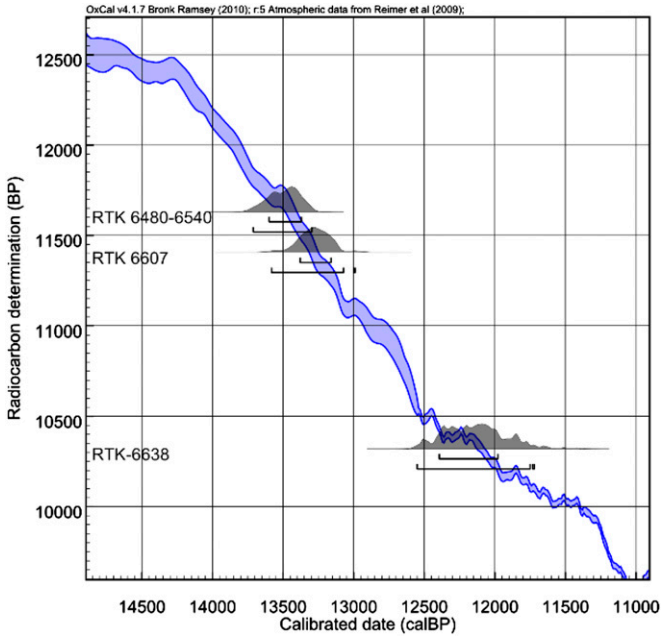

Fig. S6. Three ^{14}C dates obtained from collagen extracted from skeletons Homo 18 (RTK-6607), Homo 19 (RTK-6480-6540), and Homo 28 (RTK-6638) (following protocol of ref. 1).

1. Yizhaq M, et al. (2005) Quality controlled radiocarbon dating of bones and charcoal from the early Pre-Pottery Neolithic B (PPNB) of Motza (Israel). *Radiocarbon* 47:193–206.

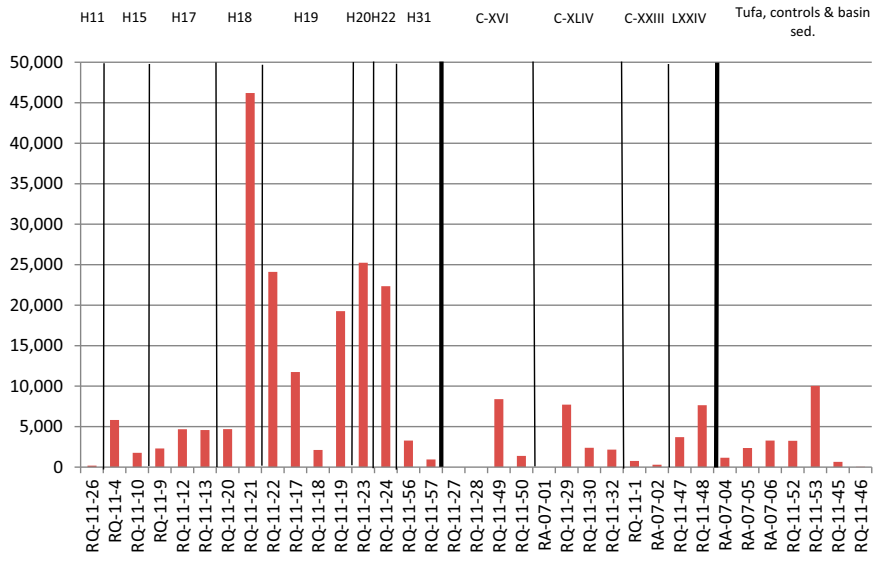

Fig. S7. The frequencies of single-cell jigsaw-puzzle phytoliths from dicot leaves. Basin sed., basin sediments; C, bedrock mortar; H, Homo.

Table S1. Data for four Natufian burials (six human skeletons) with plant impressions at Raqefet Cave

Skeleton	Posture and orientation	Age/sex	Lab no. RTK	^{14}C age ± 1σ years B.P.	^{14}C date for ± 1σ calibrated years B.P.	^{14}C date for ± 2σ calibrated years B.P.	Location of impressions in grave	No. of impressions >3 cm	Type of impressions
Homo 1	Unclear details, head to north?	Mature female			n.m.	n.m.	Bottom	>30	Square stems, seeds
Homo 18	On side, head to north	Mature female	6607	**11,405 ± 120**	13,380–13,160	13,580–13,000		Combined for both: >10	
Homo 19	On side, head to north	Young adolescent	6480, 6540	**11,725 ± 125 11,540 ± 120 Average 11,630 ± 87**	13,600–13,370	13,710–13,300	Vertical bedrock wall		Reeds? unidentified
Homo 25	On back, head to west;	Adult			n.m.	n.m.	Bottom	Combined for both: >30	*Salvia*, square stems, round stems, seeds
Homo 28	On back, head removed	Adolescent	6638	**10,320 ± 110**	12,400–11,980	12,550–11,720	Bottom, side		Square stems, round stems, wide leaves, seeds
Homo 31	On side, head to north	Child (8–10 y old)			n.m.	n.m.	Bottom, side	>6	Round stems

n.m., not measured; σ, standard deviation.

Table S2. Provenance of sediment samples analyzed for phytolith remains

Location	Sample	Grid	Locus	Depth	Feature	Description
Burials						
	RQ-11–26	C14c	3	−2.06/−2.15	Homo 11	Infant burial
	RQ-11–4	B12a	1	−2.49	Homo 15	Near tibia
	RQ-11–10	B12a	1	−2.49	Homo 15	Near tibias
	RQ-11–9	C12	1	−2.87/−2.88	Homo 17	Under thorax
	RQ-11–12	C12a–d	1	−2.85	Home 17	Under slab B4
	RQ-11–13	C12	1	−2.80/−2.82	Homo 17	Left humerus/radius
	RQ-11–20	D16	3	−2.38	Homo 18	Under stone 15 at skull and hands
	RQ-11–21	D16	3	−2.25	Homo 18	Under sacrum
	RQ-11–22	D16	3	−2.27	Homo 18	Under proximal ulna
	RQ-11–17	D16a	3	−2.20	Homo 19	Under stone 47 at abdomen
	RQ-11–18	D16c	3	−2.27/−2.28	Homo 19	Under stone 64 at proximal ulna
	RQ-11–19	D16c	3	−2.20	Homo 19	Under stone 37 at upper chest
	RQ-11–23	D14d/D15c	3	−2.06/−2.15	Homo 20	Under skull
	RQ-11–24	E15c	3	−2.16	Homo 22	Under thorax
	RQ-12–56	E14b	3	−254/−259	Homo 31	Chest area
	RQ-12–57	E14b	3	−243/−248	Homo 31	Above/near hand
Bedrock features/ mortars						
	RQ-11–27	F11d	—	46–50 cm below rim	Mortar C-XVI	
	RQ-11–28	F11d	—	50–53 cm below rim	Mortar C-XVI	
	RQ-12–49	F11d	—	53–55 cm below rim	Mortar C-XVI	
	RQ-12–50	F11d	—	55–56 cm below rim	Mortar C-XVI	
	RA-07–01	F11d	—	Base, 55–56 cm below rim	Mortar C-XVI	Sealed
	RQ-11–29	D12a	1	−2.73	Mortar C-XLIV	North wall, under Homo 9
	RQ-11–30	D12b	1	−2.69	Mortar C-XLIV	North rim
	RQ-11–32	D12b	1	−2.65/−2.70	Mortar C-XLIV	Hard internal sediment
	RQ-11–1	F12	—	5 cm above base	Mortar C-XXIII	Hard sediment
	RA-07–02	F12	—	Base of feature	Mortar C-XXIII	Hard sediment
	RQ-12–47	E14b	—	−2.50	Clay mortar LXXIV	Negative of mortar, fragment 4
	RQ-12–48	E14b	—	−2.50	Clay mortar LXXIV	Negative of mortar, fragment 6
Tufa, basin, and controls						
	RA-07–04	K7	4	−2.15/−2.27	Tufa	Late Natufian matrix
	RA-07–05	K8	4	−2.20	Tufa	Late Natufian matrix
	RA-07–06	L14a	5	−0.60/−0.70	Tufa	Kebaran matrix
	RQ-12–52	D14c	3	−2.48/−2.55	Bedrock basin	Loose sediment
	RQ-12–53	E14a	3	−2.70/−2.75	Bedrock basin	Loose sediment
	RQ-12–45	—	—	—	Control	40 m northwest of cave
	RQ-12–46	—	—	—	Control	100 m northwest of cave

Table S3. Counted phytolith morphotypes and their highest level of taxonomic identification

Phytolith morphotype	Taxonomic attribution
Single-cell phytolith morphotype	
Psilate long-cell	Grass stem
Sinuate long-cell	Grass leaves
Dendriform/echinate long-cell	Grass seed husk/inflorescence
Elongate verrucate	Grasses
Papillae	Grass inflorescences
Acicular hair	Monocots
Hairs	Monocots
Trichome	Grass leaves and inflorescences
Bulliform	Monocot leaves
Oval	Monocot stem/leaves
Crenate	Grass leaves
Short-cell bilobe	Panicoid grass stem/leaves
Polylobate	Panicoid grass stems/leaves
Short-cell rondel	Pooide grass stem/leaves/floral
Short-cell saddle	Chloridoideae grass stem/leaves
Cones	Cyperaceae stem/leaves
Stoma	Monocot
Achene type	Cyperaceae inflorescence
Platey	Dicot wood, stem and leaves
Indeterminate echinate type	Unknown taxonomical origin
Elongate	Indeterminate long cell/hair category
Tracheid	Dicot/monocot
Two-tiered	Dicot leaves
Oblong	Dicot leaves/stem
Elongate dicot wood/bark	Dicot leaves/stem
Block	Dicot leaves/stem
Smooth spheroid	Dicot
Scalloped	Dicot
Jigsaw-puzzle-shape	Dicot leaves/fruit
Multicell phytolith morphotype	
Grass cells Leaf/Stem	Monocots leaves/stems
Indeterminate husk	Indeterminate grass inflorescence
Triticum sp. husk	Wheat florescence
Hordeum husk	*Hordeum* sp. barley husk
Cf. *Hordeum*	Confer barley inflorescence
Avena husk	Cf. *Avena* (oat) inflorescence
Small seeded grass husk	Small seeded grass inflorescence of none above
Phragmites	*Phragmites* (reed) leaf and stems
Sedge stem/leaf	Sedge (Cyperaceae) leaf/stem
Sedge husk	Sedge (Cyperaceae) inflorescence
Mesophyll spheroid	Dicot and grass leaves
Stoma sheet	Monocot (commonly found in *Phragmites* leaves)
Indeterminate dicot wood/bark	Dicot wood/bark
Polyhedron	Dicot leaves
Cf. *Quercus* polyhedron	Dicot leaves
Polyhedron hair base	Dicot leaves
Scirpus husk	*Scirpus* inflorescence
Multitier: square tier	Dicot leaves
Multitier: (*Quercus*)	Dicot oak (cf. Quercus)
Jigsaw	Dicot leaves/fruit

Table S4. Density (number per gram of sediment) of select phytolith morphotypes organized by provenance

Provenance	Sample	Total phytoliths	Multicell phytoliths	Jigsaw puzzle phytoliths
Burials				
	RQ-11–26	42,160	113	562
	RO-11–4	56,558	0	0
	RQ-11–10	11,489	0	7
	RQ-11–9	11,412	0	0
	RQ-11–12	33,718	0	12
	RQ-11–13	42,495	0	21
	RQ-11–17	99,932	1,579	4,372
	RQ-11–19	179,066	2,283	2,344
	RQ-11–24	107,613	1,517	2,743
	RQ-11–18	43,324	1,636	894
	RQ-11–20	21,337	464	2,398
	RQ-11–21	97,504	9,087	26,823
	RQ-11–22	58,343	3,286	13,988
	RQ-11–23	113,231	1,134	5,599
	RQ-12–56	52,115	756	965
	RQ-12–57	8,893	881	0
Total		979,190	22,736	60,728
% of morphotype in grouping			52.7	91.1
Average		61,199	1,421	3,795
Bedrock features				
	RQ-11–1	2,710	6	170
	RQ-11–27	24,550	183	2
	RQ-11–28	154,612	1,151	73
	RQ-12–49	286,040	2,732	0
	RQ-12–50	305,843	4,386	1,384
	RQ-11–33	333,281	7,281	0
	RQ-11–29	30,884	366	0
	RQ-11–30	16,447	180	14
	RQ-11–1	2,710	6	170
	RQ-11–34	1,917	53	0
	RQ-12–47	65,676	464	347
	RQ-12–48	85,008	665	1,750
Total		1,309,678	17,473	3,901
% of morphotype in grouping			40.5	5.9
Average		109,104	1,456	3,910
Tufa and controls				
	RQ-12–52	111,699	1,479	1,172
	RQ-12–53	65,374	954	568
	RQ-11–36	7,073	23	0
	RQ-11–37	30,464	217	0
	RQ-11–38	10,378	167	254
	RQ-12–45	22,228	100	0
	RQ-12–46	32,233	32	0
Total		279,449	2,972	1,994
% of morphotype in grouping			6.9	2.6
Average		39,921	424	285